at the Mt. Bachelor Observatory (MBO) during 2004–2015

Lei Zhang[a,*] and Daniel A. Jaffe[a,b]

[a] School of Science, Technology, Engineering and Mathematics, University of Washington Bothell, Bothell, WA 98011, United States

[b] Department of Atmospheric Sciences, University of Washington, Seattle, WA 98195, United States

[*] Corresponding author.

Email address: lzhang12@uw.edu.

Abstract

In this paper, we report the climatology of tropospheric ozone (O_3) and sub-micron aerosol scattering at the Mt. Bachelor Observatory (MBO, 2.8 km asl) in central Oregon, USA, during 2004–2015. The seasonal cycle for O_3 showed a bimodal pattern with peaks in April and July, while aerosol scattering (σ_{sp}) was lognormally distributed with a very high peak in August and a smaller peak in May. The mean O_3 concentrations showed positive and significant trends in all seasons except winter, with a slope of 0.6–0.8 ppbv yr^{-1}. Monthly criteria for isolating free tropospheric (FT) and boundary layer influenced (BLI) air masses at MBO were obtained based on comparison of MBO water vapor (WV) distributions to those of Salem (SLE) and Medford (MFR), Oregon, at equivalent pressure level. In all seasons, FT O_3 was, on average, higher than BLI O_3, but the seasonal patterns were rather similar. For σ_{sp} the FT mean in spring was higher, but the BLI mean in summer was significantly higher, indicating the importance of regional wildfire smoke.

To better understand the causes for the seasonal and interannual trends at MBO, we identified four major categories of air masses that impact O_3, carbon monoxide (CO) and aerosols: upper troposphere and lower stratosphere (UTLS) O_3 intrusion, Asian long-range transport (ALRT), Arctic air pollution (AAP) and plumes from the Pacific Northwest region (PNW). ALRT and PNW plumes can be further divided into wildfires (WF), industrial pollution (IP) and mineral dust (MD). Over the 12 years of

(ERs) and Ångström exponents (AEs) of aerosols were calculated for all events. The lowest slope of $\Delta\sigma_{sp}/\Delta O_3$ is a unique feature of UTLS events. PNW-WF events have the highest averages for $\Delta\sigma_{sp}/\Delta CO$, $\Delta\sigma_{sp}/\Delta O_3$ and $\Delta\sigma_{sp}/\Delta NO_y$ compared to other events. These ERs decrease during long-range transport due to the shorter residence time of aerosols compared to the other pollutants. ALRT-WF events have lower absorption AEs ($Å_{ap}$) than PNW-WF, implying that brown carbon (BrC) is generated from biomass burning but its fraction decreases during long-range transport. Signatures of ERs and AEs are useful tools to identify different plume categories. These results demonstrate the increasing impact of baseline O_3 on US air quality due to both global sources and regional wildfire events.

Keywords: tropospheric ozone; sub-micron aerosols; western US; enhancement ratios; backward trajectories; long-term trends

1. Introduction

Tropospheric ozone (O_3) and airborne particles (aerosols), especially fine particulate matter ($PM_{2.5}$ or PM_1), have significant impacts on human health and the environment (Davidson et al., 2005). O_3 plays an important role in atmospheric chemistry and the global climate (IPCC, 2014). Sulfate and other low absorption aerosols have a dominant cooling effect and partially offset warming due to aerosol absorption and greenhouse gases (GHGs) (Charlson et al., 1992; Buseck and Pósfai, 1999; IPCC, 2014). There are at least four sources of tropospheric O_3 and aerosols in the western US: upper troposphere and lower stratosphere (UTLS) intrusion, Asian long-range transport (ALRT), Arctic air pollution (AAP) and plumes from the Pacific Northwest region (PNW). In the western US, background sources of O_3 and PM are more important compared to other parts of the US (Jaffe et al., 1999; Heald et al., 2006; Zhang et al., 2009; McDonald-Buller et al., 2011). ALRT can be broadly classified into three categories: biomass burning, mineral dust and industrial pollution (Fischer et al., 2010a; Ambrose et al., 2011).

In the troposphere, O_3 comes from secondary photochemical processes involving

nitrogen oxides (NO_x nds (VOCs) plus intrusion of stratospheric air. A significant increase in springtime O_3 mixing ratios in the western North America has been observed by Cooper et al. (2010) with evidence that it is influenced by increasing precursor emissions from Asia. Lin et al. (2012) argued that much of the recent O_3 increase was driven by variability in circulation. Among the Asian sources of O_3, Siberian wildfires could also be an important contributor (Gratz et al., 2015). UTLS intrusions have also been linked to high-O_3 events in the western US, especially in springtime (Ambrose et al., 2011; Langford et al., 2012; Lin et al., 2012; Langford et al., 2017). Regional wildfires in the western US also contribute significantly to summertime O_3 enhancement (Pfister et al., 2006; Jaffe et al., 2008; Jaffe et al., 2013; Baylon et al., 2015).

Aerosol optical properties, including scattering (σ_{sp}) and absorption (σ_{ap}), are useful indicators for source identification. The wavelength dependence of σ_{sp} is parameterized using the scattering Ångström exponent ($Å_{sp}$), defined as follows (Ångström, 1929):

$$\sigma_{sp} = \lambda^{-Å_{sp}} \quad (1)$$

Because the coefficient σ_{sp} decreases with wavelength for smaller aerosol particles, $Å_{sp}$ will be larger for smaller particle distributions (Boren and Huffman, 1983). In a similar way, $Å_{ap}$ is the absorption Ångström exponent which is related to the composition, shape and mixing state of the aerosol particles, leading to size variation as well (Bergstrom et al., 2007):

$$\sigma_{ap} = \lambda^{-Å_{ap}} \quad (2)$$

Optical coefficients (σ_{sp} and σ_{ap}) together with their wavelength dependences ($Å_{sp}$ and $Å_{ap}$) reflect the differences of diverse aerosol plumes, especially between dust aerosols and combustion-generated carbonaceous aerosols (Fialho et al., 2005; Clarke et al., 2007; Yang et al., 2009; Fischer et al., 2011; Cappa et al., 2012; Cazorla et al., 2013).

The slope of a regression curve between two pollutants is known as the enhancement ratio (ER), which is an important tool for plume source apportionment.

88 3 x

89 normalized to CO is often used to identify and characterize the production or loss of
90 the pollutant in smoke plumes, especially wildfire plumes (Goode et al., 2000;
91 Bertschi et al., 2004; Honrath et al., 2004; Bertschi and Jaffe, 2005; Pfister et al., 2006;
92 Val Martin et al., 2006; Real et al., 2007; Paris et al., 2009; Alvarado et al., 2010;
93 Fischer et al., 2010b; Singh et al., 2010; Wigder et al., 2013). This method accounts
94 for air mass dilution given the simple and well understood processing of CO. Jaffe
95 and Wigder (2012) summarized reported $\Delta O_3/\Delta CO$ values for wildfire plumes
96 arranged by biome type and by plume age and found that the average $\Delta O_3/\Delta CO$ ratio
97 increases with plume age and also that tropical regions tend to have significantly
98 greater ratios compared to boreal and temperate regions. However, they also reported
99 large variability in $\Delta O_3/\Delta CO$ ratios. Wigder et al. (2013) focused on the $\Delta PM_1/\Delta CO$
100 ratio in wildfire plume events and found evidence for secondary organic aerosol (SOA)
101 production in wildfire plumes. However, they found that with longer transport time
102 PM_1 loss is greater than SOA production. Baylon et al. (2015) looked into wildfire
103 plume events and calculated multiple ERs, including $\Delta\sigma_{sp}/\Delta CO$, $\Delta O_3/\Delta CO$,
104 $\Delta NO_y/\Delta CO$, $\Delta NO_x/\Delta CO$, $\Delta NO_x/\Delta NO_y$ and $\Delta PAN/\Delta NO_y$. The correlation between
105 $\Delta O_3/\Delta CO$ and $\Delta NO_x/\Delta NO_y$ implies that the degree of NO_x oxidation is a key predictor
106 of O_3 production.

107 In this study, we report on seasonal variations and interannual trends of O_3 and
108 sub-micron aerosols at the Mt. Bachelor Observatory (MBO) in central Oregon, USA,
109 for 2004–2015. MBO has one of the longest, continuous records of free tropospheric
110 measurements in North America. Over the 12 years of observations, 177 individual
111 plume events were identified based on elevated σ_{sp}, O_3 or CO. The purpose of this
112 study is to identify background sources of O_3 and aerosols in the western US and
113 characterize each category by a series of signatures including enhancement ratios and
114 aerosol optical properties. We recognize that many plumes have multiple sources
115 associated with them (Cooper et al., 2004), but we can identify the major contributors
116 through gridded emissions for fires and industrial pollution, combined with air mass
117 backward trajectories.

2. Methodology

2.1. Site description and measurements of air pollutants

Mt. Bachelor Observatory (MBO) is located on the summit of a dormant volcano in central Oregon (43°58′39″ N 121°41′10″ W, 2763 m asl). Due to its elevation and distance from major US source regions, local pollution is relatively rare at MBO. Mixing ratios of O_3 and CO, scattering coefficient of sub-micron aerosols and meteorological parameters (e.g., air temperature, pressure, relative humidity, wind speed and direction, water vapor) have been measured from 2004 to 2015. Mixing ratios of nitrogen oxides (NO_x and NO_y), PAN and mercury as well as sub-micron aerosol scattering and absorption coefficients at multiple wavelengths have been measured during specific campaigns. Detailed instrumentation with method detection limits (MDLs) and estimated total uncertainties (Weiss-Penzias et al., 2006; Fischer et al., 2010a; Fischer et al., 2010b; Virkkula, 2010; Ambrose et al., 2011; Fischer et al., 2011; Chen et al., 2013; Baylon et al., 2015; Gratz et al., 2015; Briggs et al., 2016) is described in Table S1 in the Supporting Information (SI).

Both aerosol scattering coefficient (σ_{sp}) and absorption coefficient (σ_{ap}) are reported at ambient temperature and pressure conditions. With σ_{sp} at 450 and 700 nm and σ_{ap} at 467 and 660 nm, dimensionless intensive optical properties, including scattering Ångström exponent ($Å_{sp}$) and absorption Ångström exponent ($Å_{ap}$), can be calculated as follows:

$$Å_{sp} = -\frac{\ln\left(\sigma_{sp}^{450} / \sigma_{sp}^{700}\right)}{\ln\left(450/700\right)} \quad (3)$$

$$Å_{ap} = -\frac{\ln\left(\sigma_{ap}^{467} / \sigma_{ap}^{660}\right)}{\ln\left(467/660\right)} \quad (4)$$

The coefficients at blue and red wavelengths were utilized in the calculation of the intensive properties, whereas we use the scattering coefficients at green wavelength to calculate plume enhancements and enhancement ratios with other pollutants.

2.2. Sounding data analysis

Twice daily (0 and 12 UTC) meteorological sounding data were obtained from the

quantify the vertical distribution of water vapor (WV) concentrations. This was used to help identify free tropospheric (FT) and boundary layer influenced (BLI) air masses at MBO. Soundings from Medford, Oregon (MFR, 42.36° N, 122.86° W, 405 m asl), and Salem, Oregon (SLE, 44.91° N, 123.00° W, 61 m asl), were used to compare with the monthly MBO WV distributions at equivalent pressure level (720–740 mbar). We have used similar techniques previously but at a seasonal resolution (Weiss-Penzias et al., 2006; Fischer et al., 2010b; Ambrose et al., 2011).

Ozonesonde data from Trinidad Head, California (THD, 41.05° N, 124.15° W, 107 m asl), during 2004–2015 were obtained from the Earth System Research Laboratory (ESRL) of NOAA (http://www.esrl.noaa.gov/gmd/ozwv/ozsondes). The THD ozonesonde data are collected in the daytime (16:00–22:00 UTC, or 8:00–14:00 local time).

2.3. Backward trajectory analysis

We computed 240-hour air mass backward trajectories from MBO for every hour of identified plume events using the Hybrid Single-Particle Lagrangian Integrated Trajectory (HYSPLIT) model version 4 (Draxler and Hess, 1998). For 2004 we used meteorological data from the Eta Data Assimilation System (EDAS) (40 km × 40 km) and the Final Global Data Assimilation System (FNL) (191 km × 191 km), and for 2005–2015 we used Global Data Assimilation System (GDAS) 1° × 1° gridded meteorological data. The starting height was set to be 1800 m above ground level based on terrain height in the 1° × 1° gridded meteorological data.

2.4. Wildfire maps and gridded industrial CO emission inventories

Daily MODIS fire detection data for North America was obtained from the United States Department of Agriculture (USDA) Forest Service (http://activefiremaps.fs.fed.us/gisdata.php). Daily MODIS fire detection data for Eurasia was downloaded from the Fire Information for Resource Management System (FIRMS) of the US National Aeronautics and Space Administration (NASA) (https://firms.modaps.eosdis.nasa.gov/download). Gridded maps (0.1° × 0.1°) of

on the Hemispheric Transport of Air Pollution (HTAP) (http://www.htap.org).

2.5. Enhancement ratio analysis

For each plume event, we performed correlation analyses among gaseous pollutants (including O_3, CO, PAN, NO_x and NO_y) and σ_{sp}. Enhancement ratios were calculated by taking the slope ($\Delta Y/\Delta X$) from the reduced major axis (RMA) regression between X and Y (Baylon et al., 2015).

3. Results and Discussion

3.1. Climatology of tropospheric O_3

3.1.1. Seasonal variation of the O_3 mixing ratio

Using the 12-year database (2004–2015), we present the seasonal variation of the O_3 mixing ratio at MBO. Fig. 1 shows the distribution of O_3 mixing ratios by month. A bimodal pattern with peaks in April and July was found, which reveals the influence of ALRT, UTLS and regional wildfires in spring and summer. The monthly average O_3 mixing ratio had the highest value (50.4 ppbv) in April and the lowest (40.5 ppbv) in November. O_3 at MBO was highest in the springtime, which was influenced by both ALRT and UTLS intrusion (Weiss-Penzias et al., 2006; Cooper et al., 2010; Ambrose et al., 2011; Lin et al., 2012; Gratz et al., 2015). Enhancements in summertime O_3 at MBO were mainly from regional wildfires in the western US (Jaffe et al., 2013; Wigder et al., 2013; Baylon et al., 2015) and UTLS intrusion in early summer, although Siberian fire plumes also contribute occasionally (Ambrose et al., 2011). The contribution of each source is further discussed in Section 3.4.

3.1.2. Trends and interannual variation of the O_3 mixing ratio

Fig. 2 shows the interannual variation of O_3 by season from 2004 to 2015. From 2004 to 2015, the mean O_3 mixing ratio in spring, summer and fall increased by 0.62±0.25 ppbv yr^{-1} (r^2 = 0.38, p < 0.05), 0.66±0.27 ppbv yr^{-1} (r^2 = 0.38, p < 0.05) and 0.79±0.34 ppbv yr^{-1} (r^2 = 0.35, p < 0.05), respectively. This trend appears to be driven by Asian pollution in spring (Ambrose et al., 2011) and regional wildfires in summer and early fall (Jaffe et al., 2013; Wigder et al., 2013; Baylon et al., 2015). However,

level and 2015 has a high O_3 level (Jaffe and Zhang, 2017). The trends in the three seasons were not significant ($p > 0.05$) for the period of 2005–2014 in contrast to the trends for the entire data record from 2004 to 2015. The springtime O_3 increase was probably linked to the increase of Asian emissions (Gratz et al., 2015). The yearly 98th percentile of O_3 at MBO, reflecting the design value, had a more significant positive trend than the median (see Fig. S1 in the SI). Lin et al. (2015) summarized previous O_3 observations from sondes, lidars and aircraft campaigns in the western US during 1995–2014 and showed a significant positive trend. However, the trend significantly slowed after 2005. Interannual variations are also very important. Significant jumps of the average O_3 mixing ratio were found in the summer of 2012 and 2015. The 2012 jump was probably related to the more frequent wildfire events as indicated by higher mean CO and aerosols at MBO. It is further verified by source identification in Section 3.4. The 2015 jump was probably linked to summer wildfires and the temperature anomaly in the western US in 2015, especially June (Jaffe and Zhang, 2017).

3.2. Climatology of sub-micron aerosol scattering

3.2.1. Seasonal variation of the aerosol scattering coefficient

Fig. 3 displays the distribution of aerosol scattering coefficient (σ_{sp}, green) by month in logarithmic scale. Sub-micron σ_{sp} also has a bimodal seasonal pattern. The highest peak occurred in August followed by a smaller peak in May. Summer plume events had a more significant influence on sub-micron aerosols than spring plume events. The highest value in August was about three orders of magnitude higher than the median value. The springtime aerosols are mainly from ALRT, including biomass burning, mineral dust and industrial pollution (Fischer et al., 2010a; Fischer et al., 2011), while summertime aerosols are mostly generated from regional and Siberian wildfires (Wigder et al., 2013; Laing et al., 2016). In summer, primary aerosols from regional wildfires have more significant impacts on MBO than aerosols from long-range transport, although Siberian wildfires are also important (Laing et al.,

2016).

3.2.2. Interannual variation of the aerosol scattering coefficient

Fig. 4 shows the interannual variation of sub-micron aerosol scattering coefficient by season from 2004 to 2015. For aerosol scattering, we saw an increase only in summer but not statistically significant (r^2 = 0.32, p = 0.06). This could be driven by recent increases in wildfire activity in the western US (Jaffe et al., 2013; Wigder et al., 2013; Baylon et al., 2015). The level of aerosol scattering in summer 2015 was exceptionally high because of the frequent and large wildfire events (Laing et al., 2016).

3.3. Free tropospheric O_3 and aerosols

3.3.1. Criteria for FT and BLI air masses at MBO

At MBO daily upslope and downslope airflows cause a pronounced diurnal variation in O_3, WV, CO_2 and other pollutants (McClure et al., 2016). We used the 2010–2015 sounding data from both MFR and SLE to obtain monthly distributions of the WV concentration at the 720–740 mbar level, which is similar to the MBO pressure. This pressure level at MFR and SLE represent FT air masses as indicated by the lack of diurnal WV variability (Weiss-Penzias et al., 2006; Ambrose et al., 2011). Hourly WV data from MBO at the same period were also processed for monthly distributions. The significant diurnal change of WV suggests an influence of planetary boundary layer (PBL) on the air at MBO in daytime (Reidmiller et al., 2010; McClure et al., 2016).

A FT dataset for MBO was defined by the monthly distribution of all WV data at 720–740 mbar from the MFR and SLE soundings. We obtained a similar WV distribution from MBO by retaining the drier portion of the distribution such that the monthly averages of the MBO data and the soundings were equivalent. The cut points are referred to as the WV criteria for FT air masses at MBO, as shown in Table 1. The retained data represent FT air masses, while the non-retained data stand for BLI air masses. The BLI air is not purely boundary layer or FT air but represents a mix of the two. MBO is influenced constantly by FT air and occasionally by daytime upslope flow to the summit from the more moist PBL air (McClure et al., 2016). The seasonal

However with a monthly resolution rather than seasonal, this study contributes to a more accurate FT/BLI isolation.

3.3.2. Free tropospheric O_3

Based on the WV criteria, the O_3 mixing ratios for FT and BLI were separated and the monthly averages of each are shown in Fig. 5. There is a significant difference (5–10 ppbv) between the average O_3 mixing ratios for FT and BLI at MBO. The FT O_3 had a peak in May unlike the BLI case, but the variations and trends for FT and BLI O_3 were similar. The most significant discrepancies occurred in May and June, reflecting the influence of ALRT and UTLS O_3 intrusion. We compared seasonal tropospheric O_3 between MBO and THD (see Fig. 5). THD tropospheric O_3 has a bimodal seasonal pattern, 2–8 ppbv higher than MBO. The highest average THD O_3 mixing ratios occur in April. The significant peak of THD O_3 in August suggests a more significant impact of regional industrial pollution and/or wildfires compared to MBO. The difference between THD and MBO could be caused by large-scale transport and local photochemical condition instead of PBL influence. Fig. S2 in the SI shows the climatology of vertical velocity at 700 mbar in the US. THD exhibits a positive overall vertical velocity while MBO has a negative one. Pacific high pressure and subsidence in northern California increase O_3 at THD (Stauffer et al., 2017), while the mean negative vertical velocity indicates greater upward airflow with high WV at MBO.

3.3.3. Free tropospheric aerosols

With the WV criteria, sub-micron aerosol scattering coefficients for FT and BLI were also separated, and the monthly average σ_{sp} is shown in Fig. 6. The mean FT σ_{sp} was higher in spring, but the mean BLI σ_{sp} was significantly higher in summer. This implies that the regional wildfire smoke (at lower elevation) in summer had more influence on the BLI atmosphere while global sources had more impacts on the FT air masses in the rest of the year. The bimodal pattern was more prominent for the FT air masses than BLI air masses due to springtime ALRT in the free troposphere. The

et al. (2016) reported that 6 of 19 biomass burning events at MBO during August 2015 were influenced by Siberian fires originating near Lake Baikal. The next section provides more evidence on the contribution of Siberian wildfires in summer.

3.4. Plume event identification

To verify the pollution sources that cause the seasonal patterns and interannual trends of O_3 and σ_{sp}, we identified plume events using hourly data of σ_{sp}, O_3 or CO that are above the 97.5 percentile of the annual dataset. The identified hours are called "polluted hours". A group of no less than eight consecutive polluted hours, plus two hours before and two hours after, was identified as a plume event (i.e., one event is at least 12 hours long). We referred to the pollutants that are enhanced for each event as the trigger pollutants. Based on these criteria, a total of 177 plume events were identified during 2004–2015. It should be noted that most plumes have multiple sources.

Based on backward trajectories and correlation between WV and O_3, plume events at MBO can be broadly classified into four categories: upper troposphere and lower stratosphere (UTLS) O_3 intrusion, Asian long-range transport (ALRT), Arctic air pollution (AAP), and plumes from Pacific Northwest (PNW). UTLS events have trajectories derived from higher elevation (5000–10000 m agl). ALRT events have longer trajectories, often tracing back to Siberia, Mongolia, China or Japan. AAP events have trajectories passing through the Arctic at lower elevations. PNW events have shorter trajectories that originate from the Pacific Northwest region at low elevation. Fig. 7a exhibits the WV-O_3 relationships for the THD sounding data (1997–2017). WV and O_3 are overall negatively correlated. The negative slope of $\Delta O_3/\Delta WV$ is steeper at higher elevations. MBO data showed a similar pattern as the THD data (Fig. 7b) which can be used for source identification. UTLS and ALRT events originate from higher elevations, and thus have higher O_3 and lower WV with steeper $\Delta O_3/\Delta WV$ slopes. The WV concentrations of these two categories are usually lower than 3 g kg^{-1}, while those of PNW events are usually higher than 4 g kg^{-1}. UTLS and

often climb up and back down over the Pacific Ocean entraining UTLS air masses. Besides backward trajectories, we used the CO level to make a rough separation. When the mean CO is in the range of 110–130 ppbv, it is considered as a mixture of UTLS and ALRT. CO level below this range implies the dominant contribution of UTLS while above this range ALRT. In either case, it is difficult to separate source of O_3 for an air parcel transported at high elevations.

ALRT and PNW events can be further categorized into wildfires (WF), industrial pollution (IP) and mineral dust (MD). Backward trajectories, wildfire detection maps from MODIS and gridded industrial CO emission inventories from HTAP were used for identifying these sub-categories. For ALRT events, an air mass may pass through fire spots, an industry-intensive region (e.g., China, Japan) or a desert region (e.g., Mongolia) at low elevation (<3000 m agl). This would carry the air pollution from all of these sources. ALRT events are usually mixed events, but we can identify which is the major contributor among WF, IP and MD. ALRT-MD has elevated σ_{sp} but low CO. However, it is much more difficult to distinguish ALRT-WF from ALRT-IP. To identify the dominant source, we estimate the CO emission rates of WF and IP in the grid boxes through which the trajectories pass to determine their relative contribution.

The backward trajectories from MBO back to East Asia have uncertainties of up to 1000 kilometers (Draxler and Hess, 1998). Therefore, we partitioned the East Asia region into 10° × 10° grids and identify those grids where the air mass passes through at low altitude (<3000 m agl) as “influential grids”. Based on the industrial CO emission inventory in 2010 from HTAP, we calculated the average CO emission rate of each grid. Fig. S3 in the SI shows the industrial CO emission rates of all grids in East Asia. The grid containing the North China Plain region (Beijing, Tianjin, Hebei, etc.) has the highest industrial emission rate (1024 kg CO s^{-1}). Wildfire maps for the East Asia region seven days (average transport time) before each event were obtained from the MODIS data. We calculated the CO emission rate from wildfires for each fire spot based on the fire radiative power (FRP) using the following equation adopted from Kaiser et al. (2012):

$$r = \kappa_l \cdot \beta_l \cdot \mathrm{FRP} \quad (5)$$

where r is the emission rate of CO, g CO s^{-1}; κ_l is the emission factor of CO that is land cover type dependent, g CO kg^{-1} (dry matter); β_l is the conversion factor that is also land cover type dependent, kg (dry matter) MJ^{-1}; FRP is the fire radiative power from the MODIS dataset, MW; l is the land cover type, including extratropical forest (EF), tropical forest (TF), savannah (SA), agriculture (AG), and so on. κ_l and β_l are from the study of Kaiser et al. (2012), and land cover information is from the MODIS data by Global Land Cover Facility (http://glcf.umd.edu/data/lc).

CO emission rates for each grid were obtained by adding up emission rates of all fire spots in the grid. We used the ratio of wildfire/industrial (W/I) CO emission rates in the influential grids to quantify the largest source. Fig. 8 shows the CO emission rates and W/I ratios of an ALRT-WF event and an ALRT-IP event. If the W/I ratio of an ALRT event is higher than 2, it is regarded as an ALRT-WF event; if lower than 0.5, it is regarded as an ALRT-IP event; and if the W/I ratio is in the range of 0.5–2, it is considered a mixing event (ALRT-WF/IP). Most events with influential grids in Siberia are ALRT-WF events, while most events with influential grids in China are ALRT-IP events.

Most PNW events are PNW-WF with a high slope of $\Delta\sigma_{sp}/\Delta\mathrm{CO}$. Air masses of PNW-IP events usually occur when regional wildfires are absent and the air mass circulates in an industry-intensive area with a long residence time in the western US at low elevation (<1000 m agl). Air masses of PNW-MD events are from the desert areas in the southwestern US with elevated σ_{sp} but low CO. PNW-IP and PNW-MD are rare events at MBO.

Fig. 9 shows the distribution of different types of plume events during 2004–2015 by month. UTLS events occur most frequently in spring and early summer. ALRT events have the highest frequency in spring with a few in summer, mainly Siberian wildfire events. PNW events mainly occur in summer and early fall.

3.5. Characteristics of typical plume events

Table S2 in the SI shows a summary of all 177 plume events. Six typical plume events

PNW-IP. Backward trajectories of these events are shown in Fig. 10. WV-O_3 and CO-σ_{sp} relations of these events are shown in Figs. S4–S9 in the SI. Means and maximum values of hourly σ_{sp}, O_3, CO, NO_x, PAN, NO_y and WV of these events are shown in Table 2.

3.5.1. Event 138: 21 July 2013 (UTLS)

Event 138 occurred at 4:00–20:00 UTC on July 21, 2013. In this event, O_3 was the only elevated compound, while CO and σ_{sp} were both at very low levels. O_3 was negatively correlated with WV ($R^2 = 0.84$). This event had the lowest hourly average of WV (1.20 g kg^{-1}) among the six events. The trajectories came from a very high altitude above the Pacific Ocean (Fig. 10a). Fig. S10 in SI shows the geopotential height at 850 mbar from the National Centers for Environmental Prediction (NCEP) Reanalysis for the East Pacific and North America region on 15 July 2013. We observe the confrontation of high and low pressure zones above the East Pacific region, which is the primary driving force of UTLS intrusion.

3.5.2. Event 151: 19 April 2014 (ALRT-WF)

Event 151 occurred between 2:00–18:00 UTC on April 19, 2014. The average σ_{sp} rose up to a maximum hourly average of 39.7 Mm^{-1}, and CO and O_3 elevated to high levels. There were significant positive correlations between σ_{sp} and CO ($R^2 = 0.93$) and between σ_{sp} and O_3 ($R^2 = 0.45$). The hourly average WV (2.45 g kg^{-1}) was lower than regional events. Air mass trajectories traveled at low elevation through an intensive wildfire region at the eastern junction of Siberia and China on April 11–13 (Fig. 10b). Fig. S11 in the SI shows the CALIPSO lidar vertical profiles one day before arrival at the western US on April 19. Polluted dust and cloud were observed in the profiles. The W/I ratio of this event was 5.28.

3.5.3. Event 148: 20–21 November 2013 (ALRT-IP)

Event 148 took place in 2013 from 21:00 on November 20 to 11:00 on November 21 (UTC). CO and σ_{sp} were enhanced in the plume. O_3 was at a low level. There were significant positive correlations between σ_{sp} and CO ($R^2 = 0.91$) and between O_3 and

CO (R^2

which was an industry-intensive region (Fig. 10c). This path avoided wildfire intensive regions and carried with it heavy industrial pollution. The CALIPSO profiles show the arrival of this event in the western US on November 21 (Fig. S12 in SI). ALRT-IP air masses frequently experience cloud processing during transport, which will reduce the amount of aerosols but not the CO. The W/I ratio of this event was 0.06.

3.5.4. Event 102: 1 May 2011 (ALRT-MD)

Event 102 occurred at 3:00–15:00 UTC on May 1, 2011. The σ_{sp} and O_3 levels were both elevated, but CO remained low. This is typical for ALRT-MD events, which are often mixed with UTLS air. Positive correlation between O_3 and σ_{sp} was observed (R^2 = 0.54). Trajectories traveled at low elevation through the Gobi Desert region in South Mongolia and North China, carrying a significant amount of mineral dust (Fig. 10d). Fig. S13 in the SI shows the CALIPSO profiles at the arrival section in the western US on May 1, and the profiles corroborate the presence of mineral dust.

3.5.5. Event 123: 25–26 August 2012 (PNW-WF)

Event 123 took place in 2012 from 11:00 on August 25 to 22:00 on August 26 (UTC). Extremely high maximum hourly values of σ_{sp} (407 Mm^{-1}) and CO (707 ppbv) were found in this event with a very strong correlation (R^2 = 0.97). NO_x and NO_y were also enhanced significantly to maximum hourly values (577 and 4648 pptv, respectively). Fig. 10e shows the local trajectories in the western US. Low-altitude trajectories traveled through two hotspots of wildfires with high FRP values in northern California on August 25–26.

3.5.6. Event 53: 25 May 2007 (PNW-IP)

Event 53 occurred at 7:00–18:00 UTC on May 25, 2007. In this event, O_3 was enhanced with an hourly average of 64.0 ppbv while CO was not (an hourly average of 124 ppbv). Trajectories circulated at low altitude above the Pacific Ocean and traveled through western Oregon to MBO without impact of wildfires (Fig. 10f). WV was also greater than the FT cutoff value. Urban pollution from industries and mobile

probably the major contributors. Trajectories for this event were originated from subtropical latitudes where background O_3 is lower, indicating the contribution from local sources.

3.6. Signatures of different event categories

Table 3 shows the mean enhancement ratios (ERs) and the aerosol Ångström exponents of different event types. These are important signatures for source identification. PNW-MD events have little data available and are thus not listed in Table 3.

3.6.1. UTLS

UTLS events have steep negative $\Delta O_3/\Delta WV$ slopes (−10.05±3.26 ppbv kg g^{-1}), which reveals that an anomalously low WV level is usually linked to a strong O_3 intrusion. UTLS and UTLS/ALRT events also have the only negative average $\Delta\sigma_{sp}/\Delta O_3$ among all event types. The $\Delta O_3/\Delta CO$ slope varies significantly among different UTLS events. UTLS events have higher $\Delta NO_x/\Delta PAN$ (0.96±0.64 pptv $pptv^{-1}$) than PNW-WF events. However, due to limited available data, this comparison should be interpreted with caution. The high $Å_{sp}$ in UTLS events should be interpreted with caution as well given the extremely low scattering coefficients.

3.6.2. ALRT-WF

ALRT-WF events have the highest $\Delta O_3/\Delta CO$ among all event types (0.52±0.64 ppbv $ppbv^{-1}$), which is caused by the large amount of O_3 precursors generated from wildfires and the long transport time for secondary O_3 generation. ALRT-WF and ALRT-WF/IP events have lower $Å_{ap}$ levels (1.45±0.02 and 1.54±0.39) than PNW-WF events (1.81±0.59), which implies that brown carbon (BrC) is generated from the biomass burning process but its fraction decreases during the long-range transport due to photobleaching (Laing et al., 2016). O_3 from Siberian wildfires can be an important influence on US surface air quality (Jaffe, 2004).

3.6.3. ALRT-IP

464 σ_{sp}

465 due to the high level of CO in industrial pollution. The $\Delta O_3/\Delta CO$ slope of ALRT-IP
466 events (0.21±0.50 ppbv ppbv^{-1}) is higher than PNW-WF but lower than ALRT-WF.
467 The long-range transport gives ALRT-IP events sufficient time for O_3 generation.
468 ALRT-IP events have a less steep negative $\Delta O_3/\Delta WV$ (−7.88±6.26 ppbv kg g^{-1}) than
469 other ALRT events, because ALRT-IP events are usually linked to cloud process
470 during transport resulting in higher WV. ALRT-IP events have the lowest average $\AA_{sp}$
471 (2.02±0.20) among all types of events, indicating relatively larger particle size. This is
472 possibly due to mixing with mineral dust sources during long-range transport.

473 3.6.4. ALRT-MD

474 ALRT-MD events are usually associated with UTLS. Mineral dust plumes occur in
475 drier air masses (lower WV), and the $\Delta O_3/\Delta WV$ of ALRT-MD is thus steeper
476 (−13.94±6.81 ppbv kg g^{-1}). In recent years, ALRT-MD events are rare compared to
477 large MD events that occurred in prior years (Husar et al., 2001; Jaffe et al., 2003).

478 3.6.5. AAP

479 The average $\Delta\sigma_{sp}/\Delta CO$ of AAP (0.13±0.15 Mm^{-1} ppbv^{-1}) is lower than ALRT-IP.
480 Arctic pollution reservoir originates mainly from industrial pollution. One signature of
481 AAP events is the high CO level and low oxidant level, resulting in low $\Delta O_3/\Delta CO$
482 (−0.28±0.60 ppbv ppbv^{-1}) and low $\Delta NO_y/\Delta CO$ (2.72±0.26 pptv ppbv^{-1}). However, the
483 number of events is limited to make a conclusive statement.

484 3.6.6. PNW-WF

485 PNW-WF events have the highest $\Delta\sigma_{sp}/\Delta CO$, $\Delta\sigma_{sp}/\Delta O_3$ and $\Delta\sigma_{sp}/\Delta NO_y$ among all
486 types of events (0.59±0.17 Mm^{-1} ppbv^{-1}, 10.98±13.16 Mm^{-1} ppbv^{-1} and 0.10±0.07
487 Mm^{-1} pptv^{-1}, respectively). This is a distinctive feature of PNW-WF events, where
488 aerosol is a dominant pollutant and has a shorter residence time than the gaseous
489 pollutants (CO, O_3 and NO_y) (Laing et al., 2016). PNW-WF events have a lower level
490 of $\Delta O_3/\Delta CO$ (0.10±0.12 ppbv ppbv^{-1}) than ALRT-WF events, indicating secondary O_3
491 formation during long-range transport and consistent with greater O_3 production after
492 extended transport (Jaffe and Wigder, 2012).

493 3.6.7. PNW-IP

494 Because MBO is near to the coast and has no large cities upwind, PNW-IP events at
495 MBO are relatively rare. These have a steeper negative $\Delta O_3/\Delta WV$ slope (−8.57±0.68
496 ppbv kg g^{-1}) than PNW-WF events, demonstrating a stronger inverse relation likely
497 associated with BLI/FT exchange.

498 **4. Conclusions**

499 Mixing ratios of O_3, CO, NO_x, NO_y and PAN and the optical properties of sub-micron
500 aerosols have been measured at MBO from 2004–2015. The monthly average O_3
501 distribution has a bimodal pattern with peaks in April and July. ALRT and UTLS
502 events were the main contributors of O_3 in the western US in spring, while regional
503 wildfires and UTLS contributed the most in summer with a non-negligible
504 contribution from Siberian wildfires. Regional wildfires had more significant impacts
505 on σ_{sp}, resulting in a very high peak in summer especially August. A smaller peak of
506 σ_{sp} is seen in May, likely due to ALRT. Between 2004–2015, the mean O_3 mixing ratio
507 in spring, summer and fall increased by 0.6–0.8 ppbv yr^{-1} driven by Asian pollution in
508 spring and regional wildfires in summer and early fall.

509 We used the 2010–2015 sounding WV data from MFR and SLE at equivalent
510 pressure level with MBO to separate FT and BLI air masses at MBO. At MBO, O_3 is
511 significantly higher (5–10 ppbv) in FT air compared to BLI air. The BLI mean σ_{sp} was
512 higher than the FT mean in summer while lower in other seasons, showing that the
513 regional air pollution in summer had more influence on the BLI atmosphere. O_3 at
514 MBO is slightly lower than an equivalent alternative (THD) over northern California
515 due to the large-scale synoptic patterns. The bimodal pattern of σ_{sp} was more
516 prominent for the FT air masses than BLI air masses due to springtime ALRT in the
517 free troposphere.

518 Over the 12 years of observations, we identified 177 individual plume events.
519 These can be broadly classified into four categories (UTLS, ALRT, AAP and PNW)
520 based on backward trajectories and the WV-O_3 relationship. ALRT and PNW can be
521 further divided into WF, IP and MD based on the CO level and the W/I ratio. Six

exponents, regarded as signatures of different event categories, were calculated. UTLS events have the lowest $\Delta\sigma_{sp}/\Delta O_3$ slope. PNW-WF events have the highest $\Delta\sigma_{sp}/\Delta CO$, $\Delta\sigma_{sp}/\Delta O_3$ and $\Delta\sigma_{sp}/\Delta NO_y$ among all types of events. The lower averages of ALRT-WF events indicate the sub-micron aerosol has a shorter residence time than the gaseous pollutants. The comparison of $\mathring{A}_{ap}$ between PNW-WF and ALRT-WF implies that BrC is generated from biomass burning, but its fraction decreases during the long-range transport, likely due to photobleaching.

Acknowledgements

The Mt. Bachelor Observatory is supported by the National Science Foundation (grant #AGS-1447832) and the National Oceanic and Atmospheric Administration (contract #RA-133R-16-SE-0758). We also acknowledge the critical data used in this analysis provided by NOAA, NASA, USDA, HTAP and the National Weather Service. HYSPLIT data were processed by Jonathan Hee. Editing assistance was provided by Dee Ann Lommers-Johnson. MBO data are permanently archived at the University of Washington data repository (https://digital.lib.washington.edu/researchworks).

References

Alvarado, M.J., Logan, J.A., Mao, J., Apel, E., Riemer, D., Blake, D., Cohen, R.C., Min, K.-E., Perring, A.E., Browne, E.C., Wooldridge, P.J., Diskin, G.S., Sachse, G.W., Fuelberg, H., Sessions, W.R., Harrigan, D.L., Huey, G., Liao, J., Case-Hanks, A., Jimenez, J.L., Cubison, M.J., Vay, S.A., Weinheimer, A.J., Knapp, D.J., Montzka, D.D., Flocke, F.M., Pollack, I.B., Wennberg, P.O., Kurten, A., Crounse, J., Clair, J.M.S., Wisthaler, A., Mikoviny, T., Yantosca, R.M., Carouge, C.C., Le Sager, P., 2010. Nitrogen oxides and PAN in plumes from boreal fires during ARCTAS-B and their impact on ozone: an integrated analysis of aircraft and satellite observations. Atmos. Chem. Phys. 10, 9739–9760.

Ambrose, J.L., Reidmiller, D.R., Jaffe, D.A., 2011. Causes of high O3 in the lower free troposphere over the Pacific Northwest as observed at the Mt. Bachelor Observatory. Atmos. Environ. 45, 5302–5315.

551
552 the air. Geogr. Ann. 11, 156–166.
553 Baylon, P., Jaffe, D.A., Wigder, N.L., Gao, H., Hee, J., 2015. Ozone enhancement in
554 western US wildfire plumes at the Mt. Bachelor Observatory: The role of NOx.
555 Atmos. Environ. 109, 297–304.
556 Bergstrom, R.W., Pilewskie, P., Russell, P.B., Redemann, J., Bond, T.C., Quinn, P.K.,
557 Sierau, B., 2007. Spectral absorption properties of atmospheric aerosols. Atmos.
558 Chem. Phys. 7, 5937–5943.
559 Bertschi, I.B., Jaffe, D.A., Jaeglé, L., Price, H.U., Dennison, J.B., 2004.
560 PHOBEA/ITCT 2002 airborne observations of trans-Pacific transport of ozone,
561 CO, VOCs and aerosols to the northeast Pacific: impacts of Asian anthropogenic
562 and Siberian Boreal fire emissions. J. Geophys. Res. 109, D23S12,
563 doi:10.1029/2003JD004328.
564 Bertschi, I.B., Jaffe, D.A., 2005. Long-range transport of ozone, carbon monoxide and
565 aerosols to the NE Pacific troposphere during the summer of 2003: observations
566 of smoke plumes from Asian Boreal fires. J. Geophys. Res. 110, D05303,
567 doi:05310.01029/02004JD005135.
568 Boren, C.F., Huffman, D.R., 1983. Absorption and Scattering of Light by Small
569 Particles. John Wiley, Hoboken, NJ.
570 Briggs, N.L., Jaffe, D.A., Gao, H., Hee, J.R., Baylon, P.M., Zhang, Q., Zhou, S.,
571 Collier, S.C., Sampson, P.D., Cary, R.A., 2016. Particulate matter, ozone, and
572 nitrogen species in aged wildfire plumes observed at the Mount Bachelor
573 Observatory. Aerosol Air Qual. Res., in press.
574 Buseck, P.R., Pósfai, M., 1999. Airborne minerals and related aerosol particles:
575 Effects on climate and the environment. Proc. Natl. Acad. Sci. USA 96, 3372–
576 3379.
577 Cappa, C.D., Onasch, T.B., Massoli, P., Worsnop, D.R., Bates, T.S., Cross, E.S.,
578 Davidovits, P., Hakala, J., Hayden, K.L., Jobson, B.T., Kolesar, K.R., Lack, D.A.,
579 Lerner, B.M., Li, S.-M., Mellon, D., Nuaaman, I., Olfert, J.S., Petäjä, T., Quinn,
580 P.K., Song, C., Subramanian, R., Williams, E.J., Zaveri, R.A., 2012. Radiative

581
582 Science 337, 1078–1081.
583 Cazorla, A., Bahadur, R., Suski, K.J., Cahill, J.F., Chand, D., Schmid, B., Ramanathan,
584 V., Prather, K.A., 2013. Relating aerosol absorption due to soot, organic carbon,
585 and dust to emission sources determined from in-situ chemical measurements.
586 Atmos. Chem. Phys. 13, 9337–9350.
587 Charlson, R.J., Schwartz, S.E., Hales, J.M., Cess, R.D., Coakley, J.A., Hansen, J.E.,
588 Hofmann, D.J., 1992. Climate forcing by anthropogenic aerosols. Science 255,
589 423–430.
590 Chen, H., Karion, A., Rella, C.W., Winderlich, J., Gerbig, C., Filges, A., Newberger,
591 T., Sweeney, C., Tans, P.P., 2013. Accurate measurements of carbon monoxide in
592 humid air using the cavity ring-down spectroscopy (CRDS) technique. Atmos.
593 Meas. Tech. 6, 1031–1040.
594 Clarke, A., McNaughton, C., Kapustin, V., Shinozuka, Y., Howell, S., Dibb, J., Zhou,
595 J., Anderson, B., Brekhovskikh, V., Turner, H., Pinkerton, M., 2007. Biomass
596 burning and pollution aerosol over North America: Organic components and
597 their influence on spectral optical properties and humidification response. J.
598 Geophys. Res. 112, D12S18, doi:10.1029/2006JD007777.
599 Cooper, O.R., Forster, C., Parrish, D., Trainer, M., Dunlea, E., Ryerson, T., Hübler, G.,
600 Fehsenfeld, F., Nicks, D., Holloway, J., de Gouw, J., Warneke, C., Roberts, J.M.,
601 Flocke, F., Moody, J., 2004. A case study of transpacific warm conveyor belt
602 transport: Influence of merging airstreams on trace gas import to North America.
603 J. Geophys. Res. 109, D23S08.
604 Cooper, O.R., Parrish, D.D., Stohl, A., Trainer, M., Nédélec, P., Thouret, V., Cammas,
605 J.P., Oltmans, S.J., Johnson, B.J., Tarasick, D., Leblanc, T., McDermid, I.S., Jaffe,
606 D., Gao, R., Stith, J., Ryerson, T., Aikin, K., Campos, T., Weinheimer, A., Avery,
607 M.A., 2010. Increasing springtime ozone mixing ratios in the free troposphere
608 over western North America. Nature 463, 344–348.
609 Davidson, C.I., Phalen, R.F., Solomon, P.A., 2005. Airborne particulate matter and
610 human health: A review. Aerosol Sci. Technol. 39, 737–749.

for trajectories, dispersion and deposition. Aust. Meteorol. Mag. 47, 295–308.

Fialho, P., Hansen, A.D.A., Honrath, R.E., 2005. Absorption coefficients by aerosols in remote areas: A new approach to decouple dust and black carbon absorption coefficients using seven-wavelength Aethalometer data. J. Aerosol Sci. 36, 267–282.

Fischer, E.V., Jaffe, D.A., Marley, N.A., Gaffney, J.S., Marchany-Rivera, A., 2010a. Optical properties of aged Asian aerosols observed over the U.S. Pacific Northwest. J. Geophys. Res. 115, D20209, doi:20210.21029/22010JD013943.

Fischer, E.V., Jaffe, D.A., Reidmiller, D.R., Jaegle, L., 2010b. Meteorological controls on observed peroxyacetyl nitrate at Mount Bachelor during the spring of 2008. J. Geophys. Res. 115, D03302, doi:03310.01029/02009JD012776.

Fischer, E.V., Perry, K.D., Jaffe, D.A., 2011. Optical and chemical properties of aerosols transported to Mount Bachelor during spring 2010. J. Geophys. Res. 116, D18202, doi:18210.11029/12011JD015932.

Goode, J.G., Yokelson, R.J., Ward, D.E., Susott, R.A., Babbitt, R.E., Davies, M.A., Hao, W.M., 2000. Measurements of excess O3, CO2, CO, CH4, C2H4, C2H2, HCN, NO, NH3, HCOOH, CH3COOH, HCHO, and CH3OH in 1997 Alaskan biomass burning plumes by airborne Fourier transform infrared spectroscopy (AFTIR). J. Geophys. Res. 105, 22147–22166.

Gratz, L.E., Jaffe, D.A., Hee, J.R., 2015. Causes of increasing ozone and decreasing carbon monoxide in springtime at the Mt. Bachelor Observatory from 2004 to 2013. Atmos. Environ. 109, 323–330.

Heald, C.L., Jacob, D.J., Park, R.J., Alexander, B., Fairlie, T.D., Yantosca, R.M., Chu, D.A., 2006. Transpacific transport of Asian anthropogenic aerosols and its impact on surface air quality in the United States. J. Geophys. Res. 111, D14310, doi:14310.11029/12005JD006847.

Honrath, R.E., Owen, R.C., Val Martín, M., Reid, J.S., Lapina, K., Fialho, P., Dziobak, M.P., Kleissl, J., Westphal, D.L., 2004. Regional and hemispheric impacts of anthropogenic and biomass burning emissions on summertime CO and O3 in the

641
642 doi:24310.21029/22004JD005147.
643 Husar, R.B., Tratt, D.M., Schichtel, B.A., Falke, S.R., Li, F., Jaffe, D., Gassó, S., Gill,
644 T., Laulainen, N.S., Lu, F., Reheis, M.C., Chun, Y., Westphal, D., Holben, B.N.,
645 Gueymard, C., McKendry, I., Kuring, N., Feldman, G.C., McClain, C., Frouin,
646 R.J., Merrill, J., DuBois, D., Vignola, F., Murayama, T., Nickovic, S., Wilson,
647 W.E., Sassen, K., Sugimoto, N., Malm, W.C., 2001. Asian dust events of April
648 1998. J. Geophys. Res. 106, 18317–18330.
649 Intergovernmental Panel on Climate Change (IPCC), 2014. Climate Change 2014:
650 Synthesis Report. Contribution of Working Groups I, II and III to the Fifth
651 Assessment Report of the Intergovernmental Panel on Climate Change. IPCC,
652 Geneva, Switzerland.
653 Jaffe, D., Anderson, T., Covert, D., Kotchenruther, R., Trost, B., Danielson, J.,
654 Simpson, W., Berntsen, T., Karlsdottir, S., Blake, D., Harris, J., Carmichael, G.,
655 Uno, I., 1999. Transport of Asian air pollution to North America. Geophys. Res.
656 Lett. 26, 711–714.
657 Jaffe, D., Snow, J., Cooper, O., 2003. The 2001 Asian dust events: Transport and
658 impact on surface aerosol concentrations in the U.S. Eos 84, 501–507.
659 Jaffe, D., 2004. Long-range transport of Siberian biomass burning emissions and
660 impact on surface ozone in western North America. Geophys. Res. Lett. 31,
661 L16106.
662 Jaffe, D., Chand, D., Hafner, W., Westerling, A., Spracklen, D., 2008. Influence of
663 fires on O3 concentrations in the western U.S. Environ. Sci. Technol. 42, 5885–
664 5891.
665 Jaffe, D.A., Wigder, N.L., 2012. Ozone production from wildfires: A critical review.
666 Atmos. Environ. 51, 1–10.
667 Jaffe, D.A., Wigder, N., Downey, N., Pfister, G., Boynard, A., Reid, S.B., 2013.
668 Impact of wildfires on ozone exceptional events in the western U.S. Environ. Sci.
669 Technol. 47, 11065–11072.
670 Jaffe, D.A., Zhang, L., 2017. Meteorological anomalies lead to elevated O3 in the

Kaiser, J.W., Heil, A., Andreae, M.O., Benedetti, A., Chubarova, N., Jones, L., Morcrette, J.J., Razinger, M., Schultz, M.G., Suttie, M., van der Werf, G.R., 2012. Biomass burning emissions estimated with a global fire assimilation system based on observed fire radiative power. Biogeosciences 9, 527–554.

Laing, J.R., Jaffe, D.A., Hee, J.R., 2016. Physical and optical properties of aged biomass burning aerosol from wildfires in Siberia and the Western USA at the Mt. Bachelor Observatory. Atmos. Chem. Phys. 16, 15185–15197.

Langford, A.O., Brioude, J., Cooper, O.R., Senff, C.J., Alvarez, R.J., Hardesty, R.M., Johnson, B.J., Oltmans, S.J., 2012. Stratospheric influence on surface ozone in the Los Angeles area during late spring and early summer of 2010. J. Geophys. Res. Atmos. 117, D00V06.

Langford, A.O., Alvarez, R.J., Brioude, J., Fine, R., Gustin, M.S., Lin, M.Y., Marchbanks, R.D., Pierce, R.B., Sandberg, S.P., Senff, C.J., Weickmann, A.M., Williams, E.J., 2017. Entrainment of stratospheric air and Asian pollution by the convective boundary layer in the southwestern U.S. J. Geophys. Res. Atmos. 122, 1312–1337.

Lin, M., Fiore, A.M., Cooper, O.R., Horowitz, L.W., Langford, A.O., Levy, H., Johnson, B.J., Naik, V., Oltmans, S.J., Senff, C.J., 2012. Springtime high surface ozone events over the western United States: Quantifying the role of stratospheric intrusions. J. Geophys. Res. 117, D00V22, doi:10.1029/2012JD018151.

Lin, M., Horowitz, L.W., Cooper, O.R., Tarasick, D., Conley, S., Iraci, L.T., Johnson, B., Leblanc, T., Petropavlovskikh, I., Yates, E.L., 2015. Revisiting the evidence of increasing springtime ozone mixing ratios in the free troposphere over western North America. Geophys. Res. Lett. 42, 8719–8728.

McClure, C.D., Jaffe, D.A., Gao, H., 2016. Carbon dioxide in the free troposphere and boundary layer at the Mt. Bachelor Observatory. Aerosol Air Qual. Res. 16, 717–728.

McDonald-Buller, E.C., Allen, D.T., Brown, N., Jacob, D.J., Jaffe, D., Kolb, C.E.,

Establishing policy relevant background (PRB) ozone concentrations in the United States. Environ. Sci. Technol. 45, 9484–9497.

Paris, J.D., Stohl, A., Nedelec, P., Arshinov, M.Y., Panchenko, M.V., Shmargunov, V.P., Law, K.S., Belan, B.D., Ciais, P., 2009. Wildfire smoke in the Siberian arctic in summer: source characterization and plume evolution from airborne measurements. Atmos. Chem. Phys. 9, 9315–9327.

Pfister, G.G., Emmons, L.K., Hess, P.G., Honrath, R., Lamarque, J.F., Martin, M.V., Owen, R.C., Avery, M.A., Browell, E.V., Holloway, J.S., Nedelec, P., Purvis, R., Ryerson, T.B., Sachse, G.W., Schlager, H., 2006. Ozone production from the 2004 North American boreal fires. J. Geophys. Res. 111, D24S07, doi:10.1029/2006JD007695.

Real, E., Law, K.S., Weinzierl, B., Fiebig, M., Petzold, A., Wild, O., Methven, J., Arnold, S., Stohl, A., Huntrieser, H., Roiger, A., Schlager, H., Stewart, D., Avery, M., Sachse, G., Browell, E., Ferrare, R., Blake, D., 2007. Processes influencing ozone levels in Alaskan forest fire plumes during long-range transport over the North Atlantic. J. Geophys. Res. 112, D10S41, doi:10.1029/2006JD007576.

Reidmiller, D.R., Jaffe, D.A., Fischer, E.V., Finley, B., 2010. Nitrogen oxides in the boundary layer and free troposphere at the Mt. Bachelor Observatory. Atmos. Chem. Phys. 10, 6043–6062.

Singh, H.B., Anderson, B.E., Brune, W.H., Cai, C., Cohen, R.C., Crawford, J.H., Cubison, M.J., Czech, E.P., Emmons, L., Fuelberg, H.E., Huey, G., Jacob, D.J., Jimenez, J.L., Kaduwela, A., Kondo, Y., Mao, J., Olson, J.R., Sachse, G.W., Vay, S.A., Weinheimer, A., Wennberg, P.O., Wisthaler, A., 2010. Pollution influences on atmospheric composition and chemistry at high northern latitudes: boreal and California forest fire emissions. Atmos. Environ. 44, 4553–4564.

Stauffer, R.M., Thompson, A.M., Oltmans, S.J., Johnson, B.J., 2017. Tropospheric ozonesonde profiles at long-term U.S. monitoring sites: 2. Links between Trinidad Head, CA, profile clusters and inland surface ozone measurements. J. Geophys. Res. Atmos. 122, 1261–1280.

731
732 Significant enhancements of nitrogen oxides, black carbon, and ozone in the
733 North Atlantic lower free troposphere resulting from North American boreal
734 wildfires. J. Geophys. Res. 111, D23S60, doi:10.1029/2006JD007530.
735 Virkkula, A., 2010. Correction of the calibration of the 3-wavelength Particle Soot
736 Absorption Photometer (3l PSAP). Aerosol Sci. Technol. 44, 706–712.
737 Weiss-Penzias, P., Jaffe, D.A., Swartzendruber, P., Dennison, J.B., Chand, D., Hafner,
738 W., Prestbo, E., 2006. Observations of Asian air pollution in the free troposphere
739 at Mount Bachelor Observatory during the spring of 2004. J. Geophys. Res. 111,
740 D10304.
741 Wigder, N.L., Jaffe, D.A., Saketa, F.A., 2013. Ozone and particulate matter
742 enhancements from regional wildfires observed at Mount Bachelor during
743 2004-2011. Atmos. Environ. 75, 24–31.
744 Yang, M., Howell, S.G., Zhuang, J., Huebert, B.J., 2009. Attribution of aerosol light
745 absorption to black carbon, brown carbon, and dust in China – interpretations of
746 atmospheric measurements during EAST-AIRE. Atmos. Chem. Phys. 9, 2035–
747 2050.
748 Zhang, L., Jacob, D.J., Kopacz, M., Henze, D.K., Singh, K., Jaffe, D.A., 2009.
749 Intercontinental source attribution of ozone pollution at western U.S. sites using
750 an adjoint method. Geophys. Res. Lett. 36, L11810.
751

Table captions

Table 1 Water vapor (WV) criteria for free tropospheric/boundary layer influenced (FT/BLI) air masses at MBO and average FT and BLI WV by month. The WV criteria are the cut-off values that make the MBO mean WV similar to the radiosonde data.

Table 2 Means and maximum values of hourly air pollutant concentrations for six typical plume events.

Table 3 Enhancement ratios (mean ± standard deviation) and aerosol Ångström exponents of different types of plume events based on hourly data at MBO.

761 **Table 1**

762 (FT/BLI) air masses at MBO and average FT and BLI WV by month. The WV criteria
763 are the cut-off values that make the MBO mean WV similar to the radiosonde data.

	Jan	Feb	Mar	Apr	May	Jun	Jul	Aug	Sep	Oct	Nov	Dec
WV Criteria ($g\ kg^{-1}$)	3.26	2.64	2.46	2.55	3.06	4.25	5.14	5.23	4.60	4.36	3.44	2.97
Average FT WV ($g\ kg^{-1}$)	2.07	1.76	1.85	1.98	2.30	2.94	3.36	3.66	3.05	2.75	2.20	1.96
Average BLI WV ($g\ kg^{-1}$)	3.99	3.46	3.41	3.65	4.45	5.58	6.58	6.41	5.72	5.28	4.42	3.82

764

765 **Table 2** Means and maximum values of hourly air pollutant concentrations for six typical plume events.

Event No.	Event time	Category [a]	σ_{sp} (Mm^{-1})		O_3 (ppbv)		CO (ppbv)		NO_x (pptv)		PAN (pptv)		NO_y (pptv)		WV ($g\ kg^{-1}$)	
			Mean	Max	Mean	Max	Mean	Max	Mean	Max	Mean	Max	Mean	Max	Mean	Max
138	2013/7/21 4:00 – 20:00	UTLS	0.9	1.8	74.3	86.3	84	94	148	171	50	69	–	–	1.20	1.97
151	2014/4/19 2:00 – 18:00	ALRT-WF	26.4	39.7	67.1	79.9	192	226	–	–	–	–	–	–	2.45	3.44
148	2013/11/20 21:00 – 2013/11/21 11:00	ALRT-IP	16.6	28.6	53.3	57.0	215	260	–	–	–	–	–	–	1.53	2.04
102	2011/5/1 3:00 – 15:00	ALRT-MD	4.8	6.0	70.0	77.5	129	134	–	–	–	–	–	–	1.73	3.53
123	2012/8/25 11:00 – 2012/8/26 22:00	PNW-WF	100.6	406.7	60.7	69.4	296	707	283	577	–	–	1418	4648	4.62	5.59
53	2007/5/25 7:00 – 18:00	PNW-IP	3.0	4.3	64.0	76.5	124	130	85	133	–	–	–	–	3.52	5.29

766 [a] UTLS: upper troposphere and lower stratosphere O_3 intrusion; ALRT: Asian long-range transport; PNW: Pacific Northwest pollution; WF: wildfires; IP: industrial pollution; MD:
767 mineral dust.
768

Table 3 Enhancement ratios (mean ± standard deviation) and aerosol Ångström exponents of different types of plume events based on hourly data at MBO.

Category [a]	Trigger pollutants	$\Delta O_3/\Delta WV$ (ppbv kg g^{-1})	$\Delta\sigma_{sp}/\Delta CO$ (Mm^{-1} $ppbv^{-1}$)	$\Delta\sigma_{sp}/\Delta O_3$ (Mm^{-1} $ppbv^{-1}$)	$\Delta\sigma_{sp}/\Delta NO_y$ (Mm^{-1} $pptv^{-1}$)	$\Delta O_3/\Delta CO$ (ppbv $ppbv^{-1}$)	$\Delta NO_y/\Delta CO$ (pptv $ppbv^{-1}$)	$\Delta NO_x/\Delta PAN$ (pptv $pptv^{-1}$)	$Å_{sp}$	$Å_{ap}$
UTLS	O_3	−10.05±3.26 (23/23) [b]	0.17±0.12 (9/19)	−0.14±0.12 (12/23)	0.04 (1/3)	0.04±1.53 (4/19)	10.08±1.80 (2/3)	0.96±0.64 (4/5)	2.66±0.88 (10)	(0)
UTLS/ALRT	O_3	−11.06±5.01 (20/20)	0.32±0.36 (9/18)	−0.07±0.20 (5/18)	0.01 (1/5)	0.17±3.17 (5/20)	−0.10±9.52 (2/6)	0.68 (1/2)	2.15±0.18 (9)	0.91±0.74 (4)
ALRT-WF	σ_{sp}, CO	−10.53±3.85 (10/11)	0.42±0.20 (4/9)	0.48±0.71 (5/11)	(0/4)	0.52±0.64 (7/9)	−5.67±21.38 (3/3)	(0/0)	2.19±0.16 (4)	1.45±0.02 (2)
ALRT-WF/IP	σ_{sp}, CO	−10.61±3.66 (6/9)	0.23±0.13 (3/8)	0.66±0.51 (5/8)	0.05±0.03 (2/5)	0.01±0.90 (3/9)	8.14±6.90 (4/5)	(0/1)	2.23±0.30 (4)	1.54±0.39 (4)
ALRT-IP	CO	−7.88±6.26 (15/22)	0.20±0.18 (11/17)	0.51±0.86 (9/18)	−0.12 (1/5)	0.21±0.50 (13/21)	7.69 (1/4)	(0/0)	2.02±0.20 (6)	(0)
ALRT-MD	σ_{sp}	−13.94±6.81 (3/3)	−0.33 (1/3)	0.18±0.01 (2/3)	(0/0)	−1.19±0.60 (3/3)	(0/0)	(0/1)	2.07±0.05 (2)	(0)
AAP	CO	−5.85±3.40 (6/6)	0.13±0.15 (4/6)	1.39±2.40 (2/6)	0.05±0.04 (2/5)	−0.28±0.60 (3/6)	2.72±0.26 (2/5)	(0/0)	(0)	(0)
PNW-WF	σ_{sp}, CO	−5.27±5.99 (42/73)	0.59±0.17 (58/63)	10.98±13.16 (30/70)	0.10±0.07 (19/25)	0.10±0.12 (20/61)	5.83±3.11 (19/25)	0.35±0.25 (6/11)	2.16±0.20 (33)	1.81±0.59 (5)
PNW-IP	CO	−8.57±0.68 (2/3)	(0/1)	1.92 (1/3)	(0/0)	(0/1)	(0/0)	(0/0)	2.25 (1)	1.86 (1)

[a] UTLS: upper troposphere and lower stratosphere O_3 intrusion; ALRT: Asian long-range transport; AAP: Arctic air pollution; PNW: Pacific Northwest pollution; WF: wildfires; IP: industrial pollution; MD: mineral dust.

[b] The first value in parentheses gives the count of available data ($\Delta Y/\Delta X$) with considerable correlation between X and Y ($R^2 \geq 0.3$), and the second number gives the count of total available data ($\Delta Y/\Delta X$).

Figure captions

Fig. 1. Statistical distributions of the O_3 mixing ratio at the Mt. Bachelor Observatory (MBO) by month. The bottom and top of the box represent the 25th and 75th percentiles (the lower and upper quartiles, q1 and q3), respectively. The band near the middle of the box represents the 50th percentile (the median). The dot near the middle of the box represents the mean. The ends of the whiskers represent q3+1.5(q3–q1) and q1–1.5(q3–q1), respectively. The dots are outliers.

Fig. 2. Trends and interannual variations of the O_3 mixing ratio by season. The points show the mean values and the bars show the standard deviations.

Fig. 3. Statistical distributions of the sub-micron aerosol scattering coefficient at the Mt. Bachelor Observatory (MBO). The bottom and top of the box represent the 25th and 75th percentiles (the lower and upper quartiles, q1 and q3), respectively. The band near the middle of the box represents the 50th percentile (the median). The dot near the top of the box represents the mean. The ends of the whiskers represent q3+1.5(q3–q1) and q1–1.5(q3–q1), respectively. The dots are outliers.

Fig. 4. Interannual variation of the aerosol scattering coefficient by season. The points show the mean values and the bars show the standard deviations.

Fig. 5. Means of the O_3 mixing ratio for MBO free tropospheric air (MBO-FT), MBO boundary layer influenced air (MBO-BLI), MBO overall (MBO) and Trinidad Head (THD) at 720–740 mbar.

Fig. 6. Means of the sub-micron aerosol scattering coefficient for free tropospheric (FT) air, boundary layer influenced (BLI) air and overall at MBO.

Fig. 7. Water vapor-ozone (WV-O_3) relationships for (a) the Trinidad Head (THD) sounding data (1997–2017) at different elevations, and (b) different categories of events at MBO (2004–2015), including upper troposphere and lower stratosphere O_3 intrusion (UTLS), Asian long-range transport events (ALRT), the combination of UTLS and ALRT, Arctic air pollution events (AAP), and Pacific Northwest pollution events (PNW).

Fig. 8.

trajectories of (a) an Asian long-range transport wildfire (ALRT-WF) event (Event 36, 9 May 2006) and (b) an Asian long-range transport industrial pollution (ALRT-IP) event (Event 148, 20–21 November 2013). Shaded grids are influential grids where trajectories are at low altitude (<3000 m agl); the numbers above and below the line in shaded grids are CO emission rates of wildfire and industry, respectively (unit: kg s^{-1}); The W/I ratio is the ratio of wildfire/industrial CO emissions.

Fig. 9. Distribution of different types of plume events during 2004–2015 by month. (PNW: Pacific Northwest pollution; IP: industrial pollution; WF: wildfire; MD: mineral dust; AAP: Arctic air pollution; ALRT: Asian long-range transport; UTLS: upper troposphere and lower stratosphere O_3 intrusion)

Fig. 10. Backward trajectories for six typical plume events at MBO: (a) an upper troposphere and lower stratosphere O_3 intrusion (UTLS) event; (b) an Asian long-range transport wildfire (ALRT-WF) event; (c) an Asian long-range transport industrial pollution (ALRT-IP) event; (d) an Asian long-range transport mineral dust (ALRT-MD) event; (e) a Pacific Northwest wildfire (PNW-WF) event; (f) a Pacific Northwest industrial pollution (PNW-IP) event.

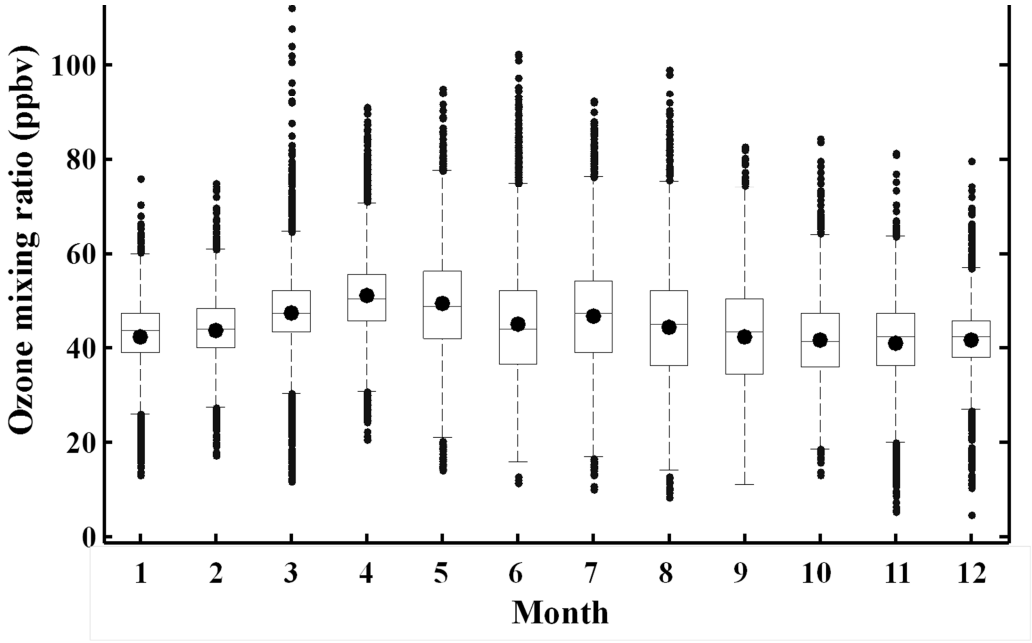

Fig. 1. Statistical distributions of the O_3 mixing ratio at the Mt. Bachelor Observatory (MBO) by month. The bottom and top of the box represent the 25th and 75th percentiles (the lower and upper quartiles, q1 and q3), respectively. The band near the middle of the box represents the 50th percentile (the median). The dot near the middle of the box represents the mean. The ends of the whiskers represent q3+1.5(q3–q1) and q1–1.5(q3–q1), respectively. The dots are outliers.

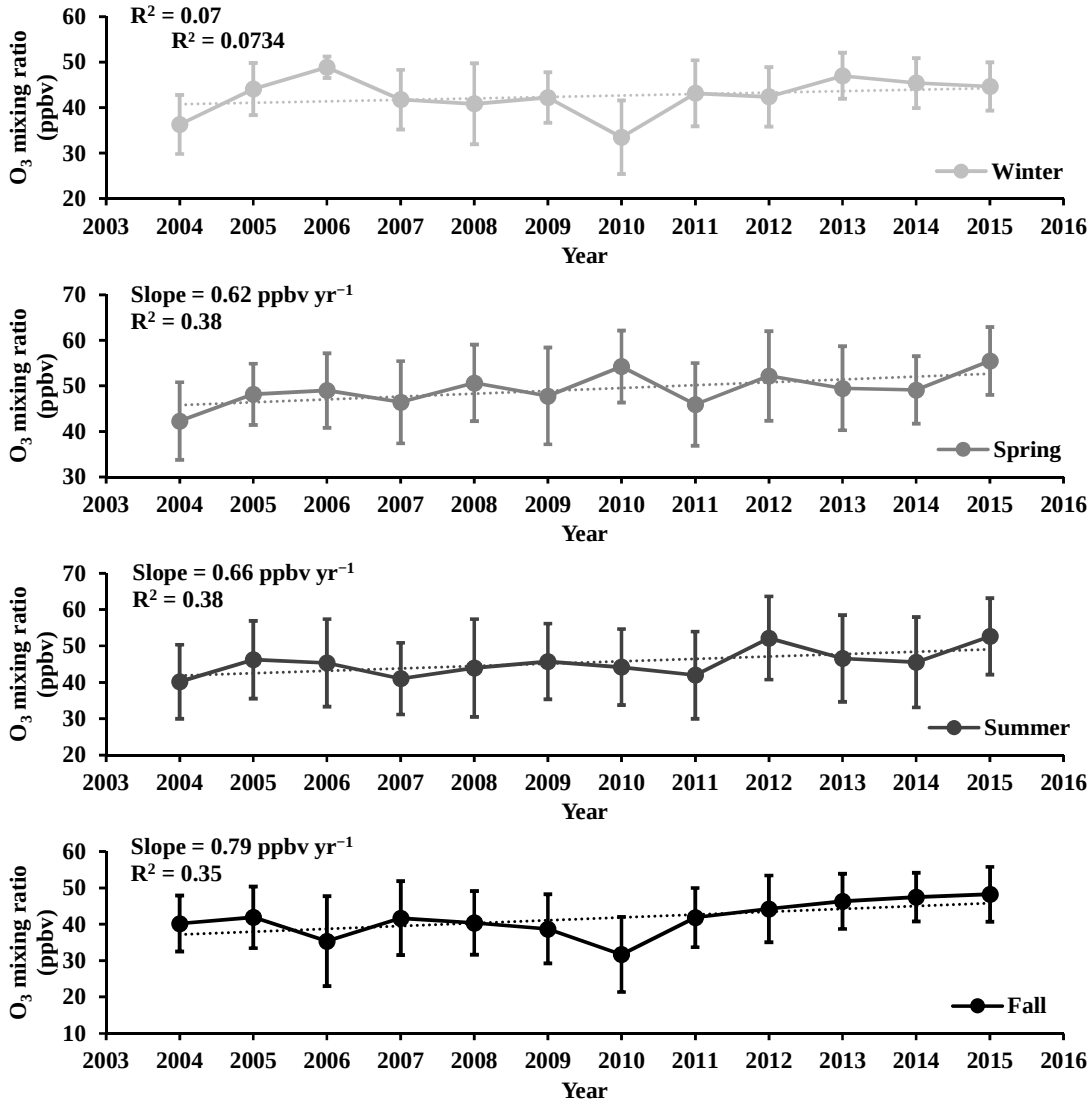

Fig. 2. Trends and interannual variations of the O_3 mixing ratio by season. The points show the mean values and the bars show the standard deviations.

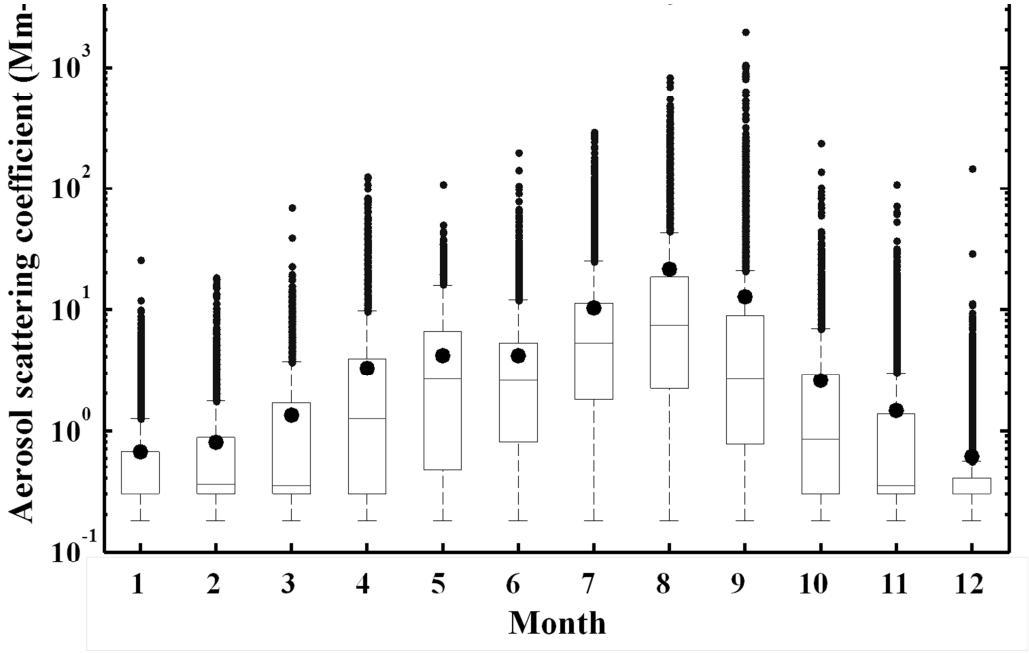

Fig. 3. Statistical distributions of the sub-micron aerosol scattering coefficient at the Mt. Bachelor Observatory (MBO). The bottom and top of the box represent the 25th and 75th percentiles (the lower and upper quartiles, q1 and q3), respectively. The band near the middle of the box represents the 50th percentile (the median). The dot near the top of the box represents the mean. The ends of the whiskers represent q3+1.5(q3–q1) and q1–1.5(q3–q1), respectively. The dots are outliers.

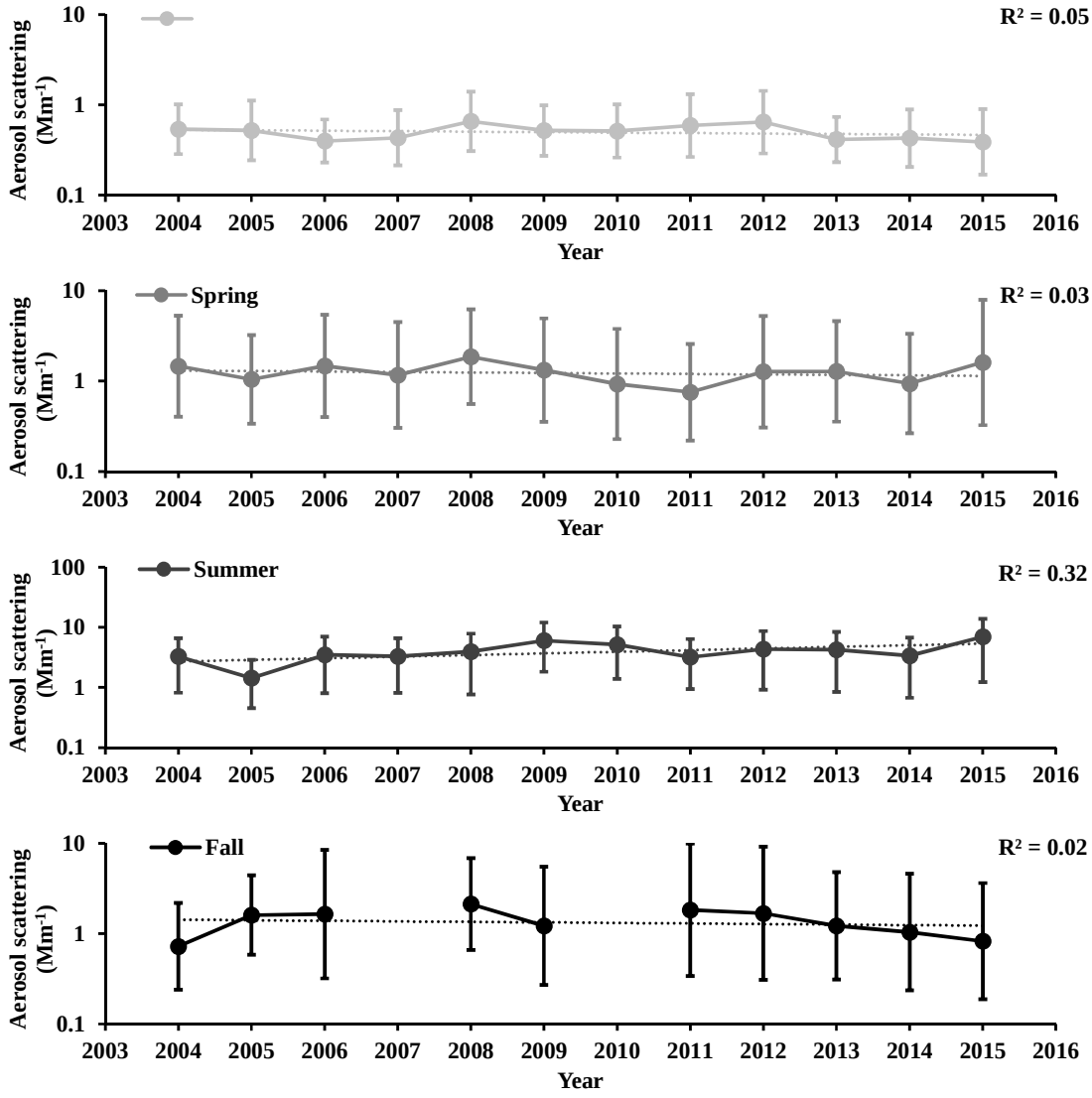

840

841 **Fig. 4.** Interannual variation of the aerosol scattering coefficient by season. The points

842 show the mean values and the bars show the standard deviations.

843

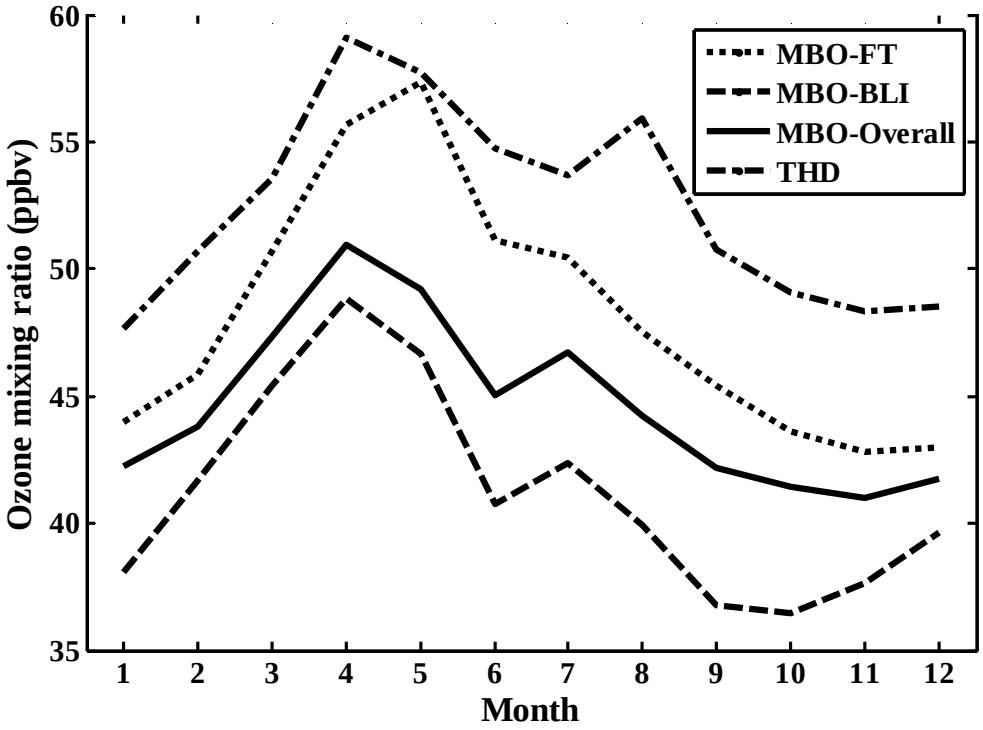

844

845 **Fig. 5.** Means of the O_3 mixing ratio for MBO free tropospheric air (MBO-FT), MBO
846 boundary layer influenced air (MBO-BLI), MBO overall (MBO) and Trinidad Head
847 (THD) at 720–740 mbar.

848

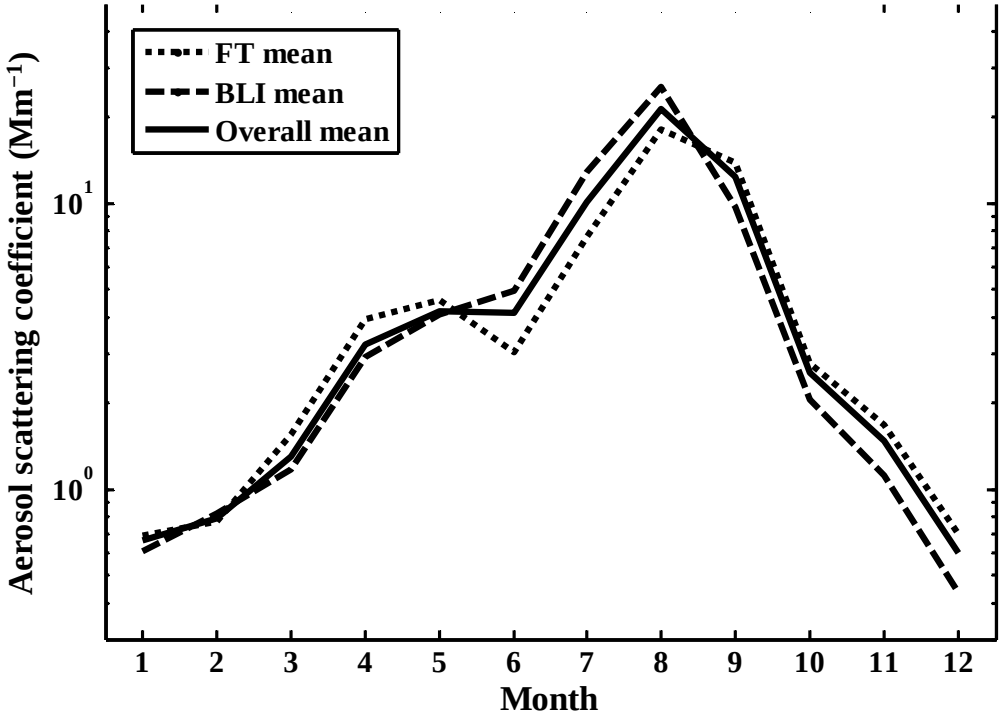

849

850 **Fig. 6.** Means of the sub-micron aerosol scattering coefficient for free tropospheric

851 (FT) air, boundary layer influenced (BLI) air and overall at MBO.

852

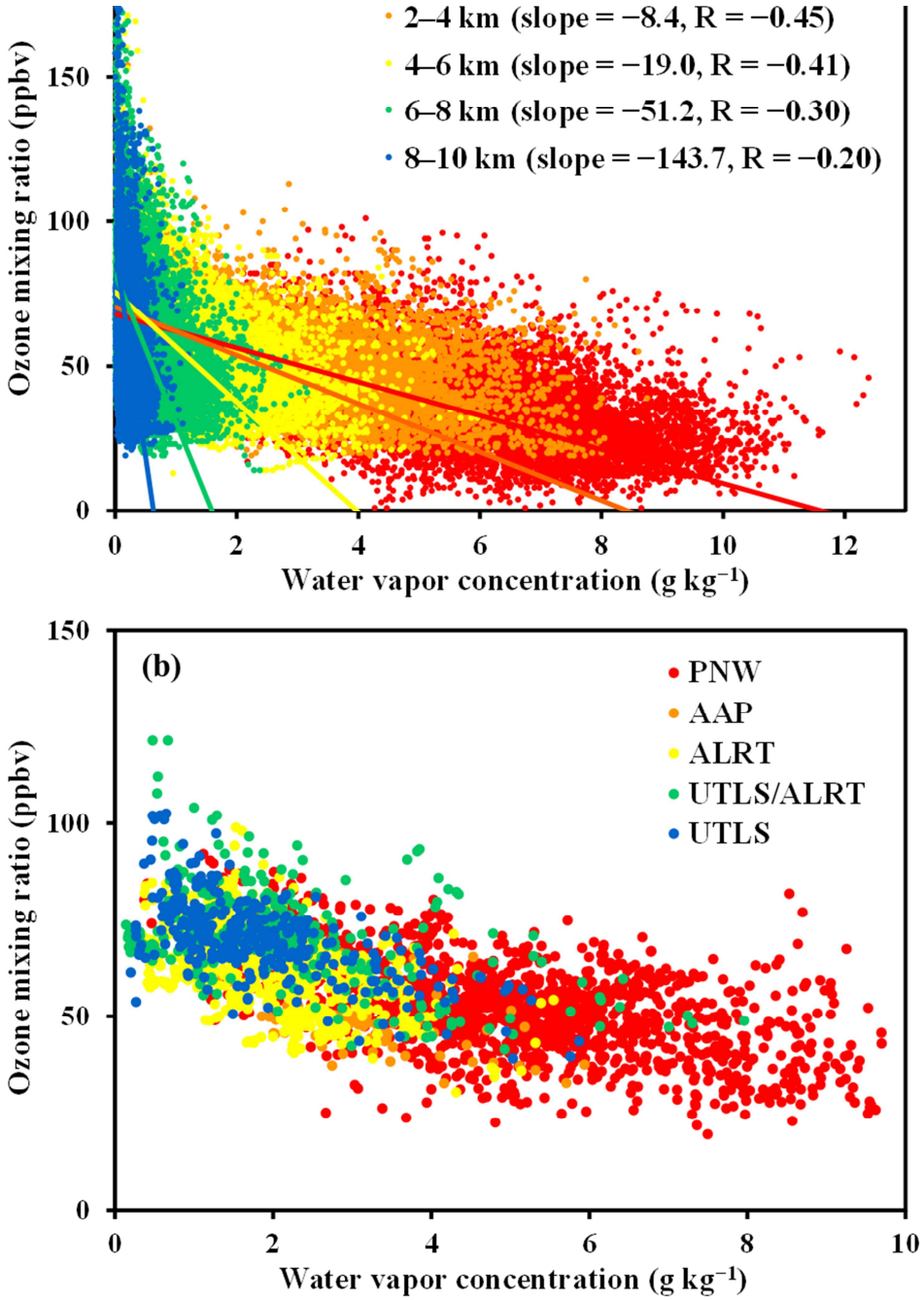

Fig. 7. Water vapor-ozone (WV-O_3) relationships for (a) the Trinidad Head (THD) sounding data (1997–2017) at different elevations, and (b) different categories of events at MBO (2004–2015), including upper troposphere and lower stratosphere O_3 intrusion (UTLS), Asian long-range transport events (ALRT), the combination of UTLS and ALRT, Arctic air pollution events (AAP), and Pacific Northwest pollution events (PNW).

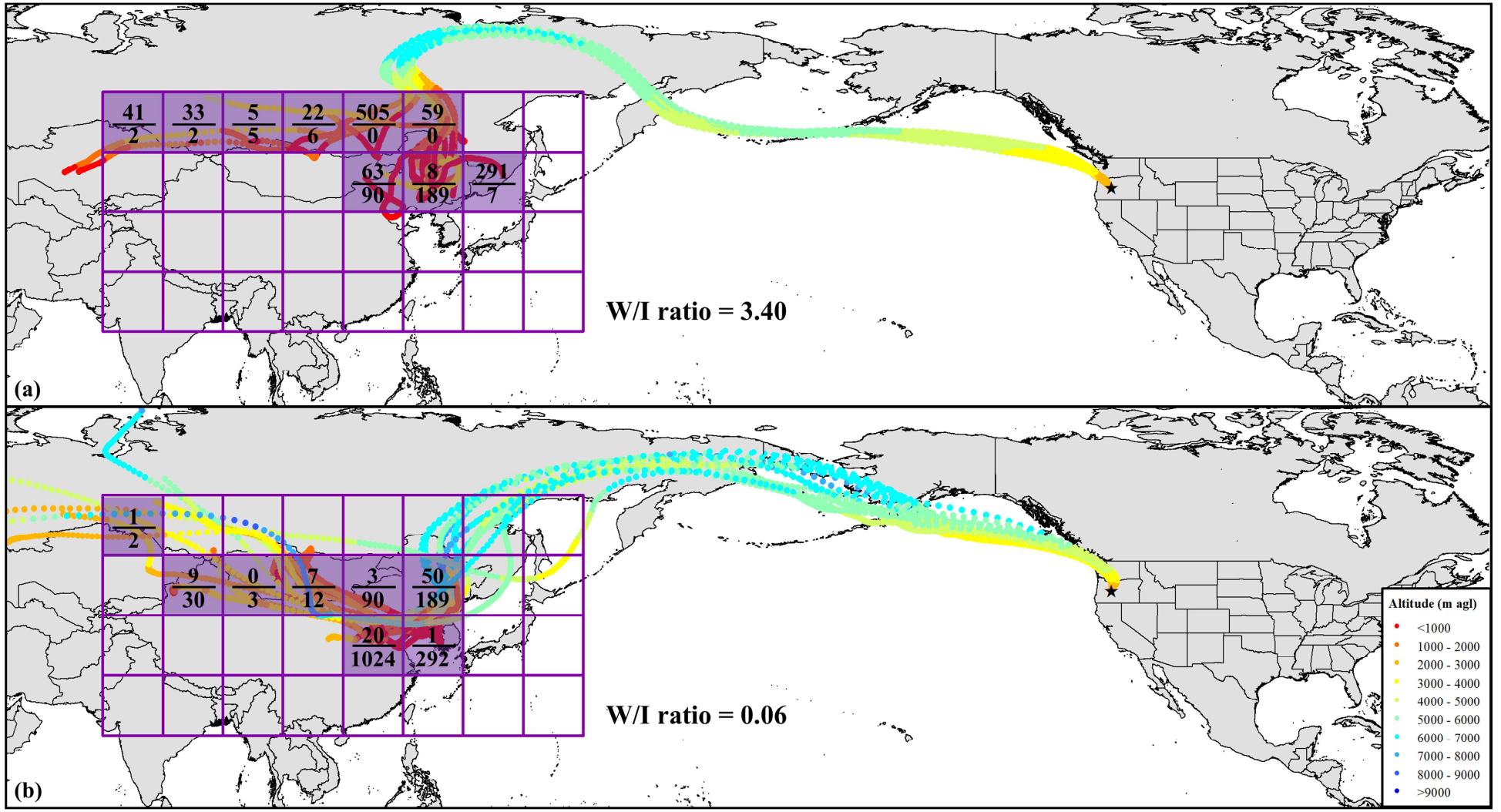

Fig. 8. Gridded East Asian carbon monoxide (CO) emission rates and HYSPLIT trajectories of (a) an Asian long-range transport wildfire (ALRT-WF) event (Event 36, 9 May 2006) and (b) an Asian long-range transport industrial pollution (ALRT-IP) event (Event 148, 20–21 November 2013). Shaded grids are influential grids where trajectories are at low altitude (<3000 m agl); the numbers above and below the line in shaded grids are CO emission rates of wildfire and industry, respectively (unit: kg s^{-1}); The W/I ratio is the ratio of wildfire/industrial CO emissions.

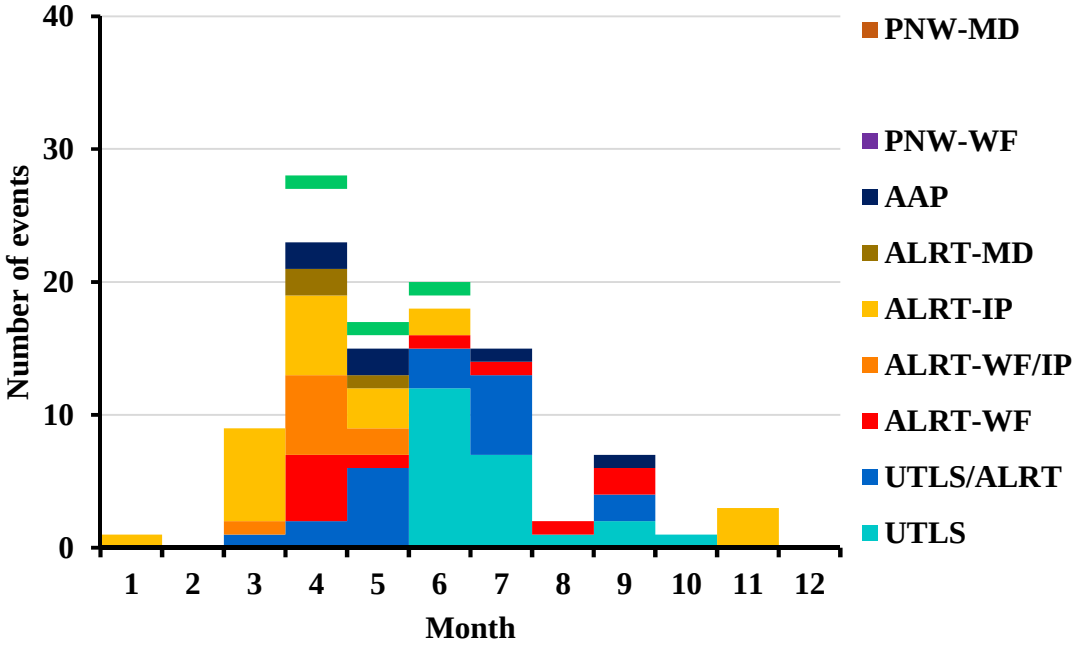

865

866 **Fig. 9.** Distribution of different types of plume events during 2004–2015 by month. (PNW:

867 Pacific Northwest pollution; IP: industrial pollution; WF: wildfire; MD: mineral dust; AAP:

868 Arctic air pollution; ALRT: Asian long-range transport; UTLS: upper troposphere and lower

869 stratosphere O_3 intrusion)

870

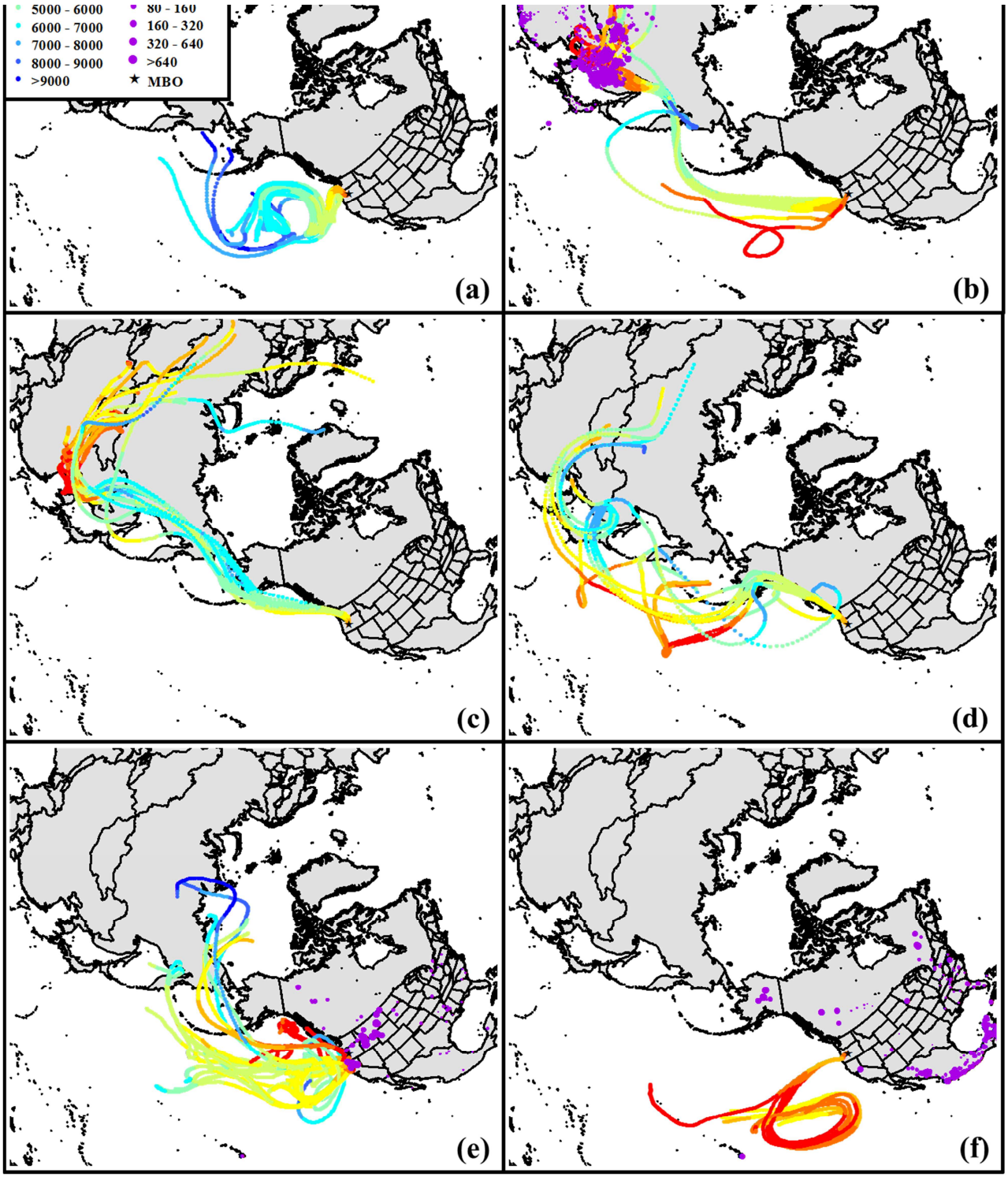

Fig. 10. Backward trajectories for six typical plume events at MBO: (a) an upper troposphere and lower stratosphere O_3 intrusion (UTLS) event; (b) an Asian long-range transport wildfire (ALRT-WF) event; (c) an Asian long-range transport industrial pollution (ALRT-IP) event; (d) an Asian long-range transport mineral dust (ALRT-MD) event; (e) a Pacific Northwest wildfire (PNW-WF) event; (f) a Pacific Northwest industrial pollution (PNW-IP) event.

1. Long-range transport and UTLS enhance tropospheric O_3 in western US in spring.
2. Interannual aerosol increase in summer is driven by regional and Siberian wildfires.
3. CO emission rate helps identify long-range transport wildfire and industrial events.
4. Enhancement ratios and aerosol optical properties provide plume event signatures.